

Explosive synchronization and hysteresis in FitzHugh-Nagumo neural networks with higher-order interactions

Wen-Xin Cao(曹文鑫), Mao-Sheng Wang(汪茂胜), Fei Xu(徐飞), Shou-Fang Huang(黄守芳), and Ji-Qian Zhang(张季谦)

Citation: Chin. Phys. B, 2026, 35 (**3**): 030503. DOI: 10.1088/1674-1056/adfc41
http://cpb.iphy.ac.cn; http://iopscience.iop.org/cpb

What follows is a list of articles you may be interested in

Optimal synchronization of higher-order Kuramoto model on hypergraphs

Chong-Yang Wang(王重阳), Bi-Yun Ji(季碧芸), and Linyuan Lü(吕琳媛)
Chin. Phys. B, 2025, 34 (**7**): 070502. DOI: 10.1088/1674-1056/adcded

Chimera states of phase oscillator populations with nonlocal higher-order couplings

Yonggang Wu(伍勇刚), Huajian Yu(余华健), Zhigang Zheng(郑志刚), and Can Xu(徐灿)
Chin. Phys. B, 2024, 33 (**4**): 040504. DOI: 10.1088/1674-1056/ad1481

Explosive synchronization of multi-layer complex networks based on star connection between layers with delay

Yan-Liang Jin(金彦亮), Qian-Yuan Han(韩钱源), Run-Zhu Guo(郭润珠), Yuan Gao(高塬), and Li-Quan Shen(沈礼权)
Chin. Phys. B, 2023, 32 (**10**): 100507. DOI: 10.1088/1674-1056/acbaf1

Explosive synchronization: From synthetic to real-world networks

Atiyeh Bayani, Sajad Jafari, and Hamed Azarnoush
Chin. Phys. B, 2022, 31 (**2**): 020504. DOI: 10.1088/1674-1056/ac3cb0

Explosive synchronization in a mobile network in the presence of a positive feedback mechanism

Dong-Jie Qian(钱冬杰)
Chin. Phys. B, 2022, 31 (**1**): 010503. DOI: 10.1088/1674-1056/ac16d3

Explosive synchronization and hysteresis in FitzHugh–Nagumo neural networks with higher-order interactions

Wen-Xin Cao(曹文鑫), Mao-Sheng Wang(汪茂胜)†, Fei Xu(徐飞),
Shou-Fang Huang(黄守芳), and Ji-Qian Zhang(张季谦)

School of Physics and Electronic Information, Anhui Normal University, Wuhu 241002, *China*

(Received 7 June 2025; revised manuscript received 27 July 2025; accepted manuscript online 18 August 2025)

This study investigates the impact of higher-order interactions on explosive synchronization and hysteresis in FitzHugh–Nagumo neural networks. We construct a higher-order network model incorporating pairwise (1-simplex) and three-body (2-simplex) interactions, along with a nonlinear coupling mechanism inspired by the Rosenzweig-MacArthur model. Using the order parameter and standard deviation as metrics, we analyze synchronization dynamics through numerical simulations. Our results demonstrate that higher-order interactions not only enhance the explosive synchronization but also induce hysteresis, with the hysteresis width growing as higher-order coupling strengthens. Furthermore, increasing noise intensity suppresses the bistability induced by higher-order interactions, ultimately eliminating hysteresis. These findings reveal the critical role of higher-order interactions in synchronization dynamics, offering theoretical insights for controlling collective behavior in neuroscience, ecology, and related fields. This work advances the understanding of synchronization in complex systems and provides new methodologies for studying multi-body interactions in real-world networks.

Keywords: higher-order interactions, explosive synchronization, hysteresis, FitzHugh–Nagumo neural network

PACS: 05.45.Xt, 05.45.–a, 87.19.lj, 89.75.Hc

DOI: 10.1088/1674-1056/adfc41 **CSTR:** 32038.14.CPB.adfc41

1. Introduction

Since Watts and Strogatz proposed the small-world network model,[1] the study of complex networks has advanced remarkably and found wide applications in physics, biology, ecology, social sciences, engineering, and other fields.[2–5] Complex networks, composed of numerous nodes and edges connecting them, can effectively represent real-world systems such as power grids, transportation networks, social networks, and neural networks. Here, nodes represent individuals in real-world systems, and edges indicate interactions or relationships between them. They provide a powerful tool for understanding and modeling interactions in complex systems.

The study of complex networks involves multiple aspects, among which the phenomenon of synchronization has received extensive attention and in-depth study.[6–8] Synchronization is an extremely common phenomenon in nature, reflecting the remarkable self-organization ability of coupled individuals and manifesting as the collective coordination and harmony of individual behaviors.[7,9] This phenomenon occurs widely in multiple fields, such as the rhythmic luminescence of fireflies and the synchronous activity of neural networks in the brain.[10] The types of synchronization phenomena are rich and diverse, including complete synchronization, phase synchronization, lag synchronization, and generalized synchronization.[9] However, synchronization transitions can also be classified by their dynamical abruptness. Unlike the continuous transitions typically observed in complete or phase synchronization, explosive synchronization[11,12] represents a discontinuous phase transition where the system abruptly jumps between incoherent and synchronized states. Crucially, explosive synchronization is usually accompanied by hysteresis: the critical coupling strength for synchronization onset during increasing coupling differs from that for desynchronization during decreasing coupling, forming a bistable region where both states coexist.[13–15] This contrasts with conventional synchronization, which exhibits no hysteresis or bistability. The bistability and rapid state switching in explosive synchronization are closely related to practical problems such as epileptic seizures and the hypersensitivity in chronic pain experienced by fibromyalgia patients.[16] Although this phenomenon has attracted extensive attention, its underlying mechanism remains unclear.

In traditional complex network research, system entities are often abstracted into nodes, and interactions between them are abstracted into edges, representing a pairwise-interaction-based modeling approach.[17] However, in the real world, interactions frequently extend beyond simple pairwise relationships. For example, in brain networks,[18] scheduling networks,[19] and computer networks,[20] interactions between individuals may involve multiple entities. Specifi-

†Corresponding author. E-mail: wangms@mail.ahnu.edu.cn

© 2026 Chinese Physical Society and IOP Publishing Ltd. All rights, including for text and data mining, AI training, and similar technologies, are reserved.

cally, a paper typically requires collaboration among several scientists,[21,22] interactions within a social group often involve multiple members,[23,24] and there exist complex competitive and cooperative relationships among organisms in ecosystems.[25] In these cases, describing the system using only pairwise interactions is clearly insufficient. Therefore, it is necessary to go beyond the pairwise interaction framework and introduce higher-order interaction network models, specifically higher-order networks.

Higher-order networks primarily adopt two representation forms: hypergraphs and simplicial complexes.[17,25,26] Hypergraphs overcome the limitation of conventional networks that only capture pairwise relationships by permitting single edges to connect multiple nodes, thereby enabling more flexible modeling of multi-body interactions in complex systems. Simplicial complexes further incorporate topological structures by organizing simplices of varying dimensions into simplicial complexes,[27,28] where an n-dimensional simplex comprises $n+1$ nodes. Specifically, a 0-simplex represents an isolated individual with one node, a 1-simplex denotes pairwise interactions with two nodes, a 2-simplex captures three-body interactions with three nodes, and a 3-simplex represents four-body interactions with four nodes. This framework effectively characterizes hierarchical relationships ranging from individual entities to complex multi-body interactions, serving as a powerful analytical tool for investigating higher-order topological properties and collective behaviors in diverse systems.

Recently, there has been growing emphasis on the importance of higher-order interactions in physics and neuroscience. Through in-depth studies of collective dynamics in higher-order networks, scientists have found that these interactions play a key role in regulating collective system behavior.[29–34] They also have wide applications in areas such as link prediction,[35] network reconstruction,[36] game theory,[37] and epidemic spreading.[38] Recent research shows they can significantly impact synchronization in complex networks, particularly by promoting explosive synchronization. For instance, Smith *et al*. used a self-consistent analysis method to study coupled oscillator synchronization in higher-order interaction networks, revealing how these interactions trigger explosive synchronization.[39] Xu *et al*. found they not only enhance synchronization but also widen the bistable region.[40] Bianconi *et al*. introduced an adaptive coupling mechanism, demonstrating how higher-order interactions induce explosive synchronization in the Kuramoto model.[41] Additionally, Skardal *et al*. studied the effects of higher-order interactions on synchronization in real-world networks, including the macaque brain network, the British power grid, and synthetic networks. They discovered that even with negative pairwise interactions, higher-order interactions can stabilize synchronous states and induce explosive synchronization.[16] These findings highlight the pivotal role of higher-order interactions in the synchronization dynamics of complex networks and provide new insights into collective behavior in complex systems.

Recent studies have highlighted the significant impact of higher-order interactions on the functionality and behavior of neural networks. For instance, Sacu[42] demonstrated that incorporating second-order interactions in fractional-order Hindmarsh–Rose neural networks significantly enhances synchronization performance compared to networks with only first-order interactions. Similarly, Li *et al*.[43] showed that in small-world networks with higher-order neural motifs, higher-order interactions can improve the response to weak signals by increasing the firing rate of output neurons. Furthermore, Yang *et al*.[44] found that higher-order interactions in fractional coupled neural networks can reduce the required coupling strength for synchronization, thereby optimizing the overall performance. These findings underscore the necessity of exploring higher-order interactions to capture the complex interdependencies in neural systems, which are often overlooked by traditional pairwise interaction models.

The FitzHugh–Nagumo (FHN) neuron model[45–47] captures the core feature of neuronal excitability (e.g., threshold-spike response) in isolated neurons. When coupled in networks, FHN neurons exhibit rich nonlinear dynamics such as chaos, multistability, and synchronized periodic firing.[45,48] Notably, excitatory or inhibitory behaviors emerge from synaptic coupling, not intrinsic to single neurons. Under traditional pairwise interaction networks, Chen *et al*. discovered explosive synchronization and hysteresis phenomena in FHN neurons.[49] However, despite the significant role of higher-order networks in complex systems, research on explosive synchronization and hysteresis in FHN neurons within higher-order networks has not yet been fully explored. Motivated by this, in the present study, we introduce higher-order interactions into a globally coupled FHN neuronal network to explore potential explosive synchronization and hysteresis phenomena in the system. Using the order parameter and standard deviation as quantitative measures, we find that the introduction of higher-order interactions not only significantly promotes the emergence of hysteresis but also leads to a marked increase in hysteresis width with stronger higher-order coupling. Subsequently, we investigate the effects of noise on explosive synchronization and hysteresis, revealing that while these phenomena remain stable under weak noise, they are disrupted under stronger noise conditions. These results demonstrate that higher-order interactions play a crucial role in explosive synchronization and hysteresis, whereas noise regulates the stability of bistability by perturbing the system state. Our findings provide new insights into the emergence mechanisms of

collective behaviors in complex systems.

2. Theoretical model

In this work, we construct a higher-order network of FHN neurons to explore how higher-order interactions affect system synchronization, compared to the traditional pairwise framework. Here, we focus on the most basic interactions in the network: pairwise (1-simplex) and three-body interactions (2-simplex). Pairwise interactions are globally coupled, so any two oscillators are connected by an edge. A 2-simplex forms when all three oscillators are connected via pairwise interactions. We do not consider higher-order simplices (e.g., 3-simplex or above) in this study. As shown in Fig. 1, in this 8-node higher-order network example, edges represent pairwise interactions. Different colors indicate three of the 21 possible 2-simplexes linked to the red node; only three are displayed for clarity.

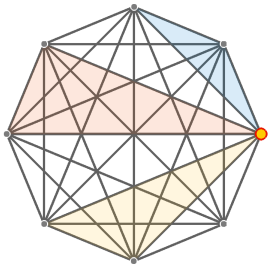


Fig. 1. A schematic diagram of a higher-order network with 2-simplexes, comprising 8 nodes.

The dynamics of the coupled FHN system can be described by the following differential equations:

$$\begin{aligned}\varepsilon_i \dot{x}_i &= x_i - \frac{x_i^3}{3} - y_i + \frac{k_1}{\langle k^1 \rangle}\sum_{j=1}^{N} A_{ij}(x_j - x_i) \\ &\quad + \frac{k_2}{\langle k^2 \rangle}\sum_{j=1}^{N}\sum_{k=1}^{N} B_{ijk}(x_j^2 x_k - x_i^3), \qquad (1)\\ \dot{y}_i &= x_i + b + \sqrt{2D}\xi_i(t). \qquad (2)\end{aligned}$$

Here, x_i and y_i denote the membrane potential and recovery variable of the i-th FHN neuron, where $i = 1, 2, \ldots, N$ and N is the total number of neurons in the network. Unless otherwise specified, the network size was fixed at $N = 101$ neurons throughout this study. k_1 and k_2 are the coupling strengths for pairwise and three-body interactions, respectively. While negative pairwise coupling ($k_1 < 0$) represents idealized repulsion, it captures essential inhibitory mechanisms including lateral inhibition and homeostatic synaptic depression, which facilitate bistability and enable abrupt synchronization transitions in neural systems. $\langle k^1 \rangle$ and $\langle k^2 \rangle$ represent the average degrees of 1-simplexes and 2-simplexes. A_{ij} is the adjacency matrix with $A_{ij} = 1$ if there is a pairwise interaction between node i and j, and $A_{ij} = 0$ otherwise. B_{ijk} is the second-order adjacency tensor, defined as $B_{ijk} = 1$ if there is a three-body interaction among nodes i, j, and k, and $B_{ijk} = 0$ otherwise. In this study, we use globally coupled pairwise interactions. The network contains $N(N-1) = 10100$ 1-simplexes and $N(N-1)(N-2) = 999900$ 2-simplexes. The number of 2-simplexes is significantly large. The average degree of 1-simplexes $\langle k^1 \rangle$ is $N-1$, and the average degree of 2-simplexes $\langle k^2 \rangle$ is $(N-1)(N-2)$. In traditional research, pairwise interactions typically adopt linear coupling, and most higher-order interaction models also follow the linear assumption.[50,51] Linear coupling assumes that the interaction between two nodes is directly proportional to the difference in their states, which can be expressed as for pairwise interactions. This approach simplifies the analysis but may not capture the full complexity of real-world interactions, especially when multiple entities are involved. In contrast, the nonlinear coupling mechanism used in this study, inspired by the Rosenzweig–MacArthur predator-prey model,[52,53] incorporates nonlinear terms to more realistically simulate saturation effects or competitive feedback in many-body synergy. This approach allows for more complex and realistic dynamics, which are essential for understanding the behavior of higher-order interactions in neural networks. The parameter ε_i is the timescale separation parameter that ensures the dynamics of the membrane potential x_i evolve significantly faster than those of the recovery variable y_i, with ε_i typically satisfying $\varepsilon_i \ll 1$. In this study, ε_i takes a random value between 0.005 and 0.007. The deterministic bifurcation parameter b governs the system's dynamical regime: when $|b| < 1$, the system exhibits sustained oscillations, whereas $|b| > 1$ leads to an excitable state. To maintain oscillations, we fix $b = 0.5$. The noise intensity D scales the influence of Gaussian white noise $\xi_i(t)$, which obeys $\langle \xi_i(t) \rangle = 0$ and $\langle \xi_i(t)\xi_j(s) \rangle = \delta_{ij}\delta(t-s)$.

Throughout this study, we employed the second-order Runge–Kutta method to numerically simulate the dynamical equations (1) and (2), using a time step of $\mathrm{d}t = 0.002$. The simulation was run for 1.25×10^5 iterations, with the initial 0.25×10^5 iterations discarded to eliminate transient effects before analyzing the synchronization behavior in the remaining data.

To comprehensively characterize the system's synchronization behavior, we employ two metrics: the standard deviation σ and the order parameter r. These two metrics provide complementary perspectives on synchronization behavior — amplitude synchronization and phase synchronization respectively — thereby offering a comprehensive characterization of the system's synchronization properties. The expression for

$\sigma(t)$ is given by

$$\sigma(t) = \sqrt{\frac{\sum_{i=1}^{N}(x_i(t) - \langle x(t)\rangle)^2}{N}}, \tag{3}$$

$$\langle x(t)\rangle = \frac{1}{N}\sum_{i=1}^{N} x_i(t). \tag{4}$$

Here, $\langle x(t)\rangle$ represents the mean value of the system's state variables at time t, while $\sigma(t)$ quantifies the dispersion of oscillator amplitudes at time t. The time-averaged value $\sigma = [\sigma(t)]$ serves as a statistical measure: when σ approaches zero, the system achieves complete synchronization; larger σ values indicate weaker synchronization. The order parameter $r(t)$ is defined as

$$r(t) = \frac{1}{N}\left|\sum_{i=1}^{N} \mathrm{e}^{-\mathrm{i}\theta_i(t)}\right|, \tag{5}$$

$\theta_i(t)$ with the phase of the i-th oscillator given by

$$\theta_i(t) = \tan^{-1}\left(\frac{y_i(t)}{x_i(t)}\right). \tag{6}$$

Here, $\theta_i(t)$ denotes the phase of the i-th oscillator at time t, and $r(t)$ measures the phase coherence among oscillators. The time-averaged order parameter $r = [r(t)]$ ranges between 0 and 1: when $r = 1$, the system achieves perfect phase synchronization; when $r \approx 0$, the system is in a completely incoherent state. To quantify the statistical variability, all results presented in the figures (e.g., Figs. 2, 5, 6) include error bars representing the standard deviation computed over 10 independent simulation runs for each parameter configuration.

3. Numerical results

First, ignoring noise ($D = 0$), we investigated system synchronization behavior under different three-body interaction strengths k_2 through forward and backward simulations (gradually increasing and decreasing k_1, respectively). Specifically, with k_2 fixed at 0, 0.25 and 0.6, we plotted the curves of both the order parameter r and standard deviation σ against the pairwise interaction strength k_1. In the simulations, k_1 was initially increased from -1.2 to 0.2 in increments of $\Delta k_1 = 0.025$, then subsequently decreased back to -1.2 using the same step size. To ensure continuity in the system evolution, the final state of each simulation served as the initial condition for the subsequent one.

As shown in Fig. 2, when higher-order interactions are absent in the system, the synchronization transition exhibits a critical abrupt change from the incoherent state to the synchronized state, representing a typical explosive synchronization phenomenon. In this case, the forward and backward simulation curves nearly completely overlap. This indicates that during both increasing and decreasing coupling strength, the critical transition points between incoherent and synchronized states coincide, with no observable hysteresis effect. With the introduction of higher-order interactions at $k_2 = 0.25$, the forward simulation shows an abrupt transition from the incoherent to synchronized state at $k_{1,\mathrm{f}}^{\mathrm{c}} = -0.35$, while the backward simulation demonstrates a reverse transition at $k_{1,\mathrm{b}}^{\mathrm{c}} = -0.45$. The mismatch between these critical points leads to curve separation and the emergence of hysteresis. When k_2 is further increased to 0.6, the hysteresis width significantly expands, with the hysteresis region shifting toward lower k_1 values. The higher-order interactions effectively reduce the threshold values for critical transitions in both forward and backward processes.

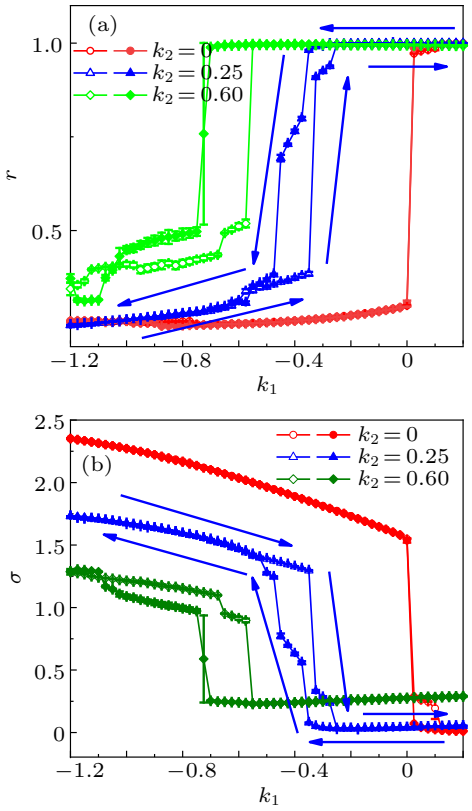


Fig. 2. The order parameter r (a) and standard deviation σ (b) as functions of pairwise interaction strength k_1. Red, blue, and green curves represent three-body interaction strengths $k_2 = 0$, 0.25, and 0.6, respectively. Other parameters: $N = 101$, $b = 0.5$, $D = 0$. Directional arrows indicate parameter scan paths: $\rightarrow$ forward (increasing k_1), $\leftarrow$ backward (decreasing k_1).

When the magnitude of k_1 falls within the hysteresis range, the system exhibits bistability. This means it can stably reside in either a synchronized or desynchronized state depending on its initial conditions. To visually demonstrate this bistability phenomenon, we selected two points corresponding to $k_1 = -0.35$ on the hysteresis curve of $k_2 = 0.25$ and generated their respective spatiotemporal sequence plots. These plots reveal distinct evolutionary differences between forward and backward simulation directions. As shown in Fig. 2, the

forward simulation displays highly irregular spatiotemporal patterns, indicating a desynchronized state. In contrast, the backward simulation exhibits remarkable regularity and coherence, demonstrating complete synchronization where oscillators operate in perfect coordination. This bidirectional transition between incoherent states and synchronization, along with direction-dependent behavioral divergence, constitutes the hallmark of bistability. It highlights the system's sensitivity to external conditions (e.g., initial states and parameter variation directions) within specific parameter ranges, while emphasizing the critical role of higher-order interactions in governing system dynamics.

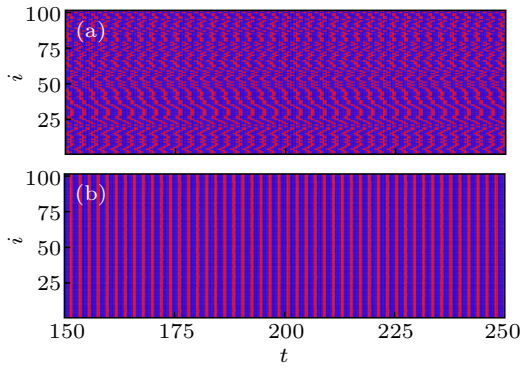


Fig. 3. Spatiotemporal sequence diagrams of the system at $k_1 = -0.35$ and $k_2 = 0.25$ in the curve of σ versus k_1: (a) forward simulation, (b) backward simulation. All other parameters remain unchanged.

In the preceding analysis, we fixed k_2 to investigate the dependence of the order parameter r and standard deviation σ on the pairwise interaction strength k_1. However, this approach captures synchronization behavior only at specific higher-order interaction strengths. To fully characterize how r and σevolve with both k_1 and k_2, we constructed their phase diagrams as functions of k_1 and k_2. Figures 4(a) and 4(d) show synchronization differences between backward and forward simulations ($\Delta r = r^{\mathrm{b}} - r^{\mathrm{f}}$, $\Delta\sigma = \sigma^{\mathrm{b}} - \sigma^{\mathrm{f}}$); figures 4(b) and 4(e) show the distribution patterns of r^{f} and σ^{f} during forward simulation. Panels (c) and (f) show distribution patterns of r^{b} and σ^{b} during backward simulation. In panels (b) and (c), red regions denote synchronized states, while remaining areas represent incoherent dynamics. In panels (e) and (f), blue regions indicate synchronized regimes, with other zones showing incoherent behavior.

In Figs. 4(a) and 4(d), regions with non-zero values correspond to the hysteresis area, flanked by zero-value zones representing the incoherent regime (lower k_1) and synchronization regime (higher k_1). Analysis of Fig. 4 reveals that for small k_2, the system requires significantly larger k_1 values to achieve synchronization. However, as k_2 increases, the critical k_1 thresholds for synchronization-incoherence transitions in both backward and forward simulations markedly decrease. Notably, the synchronization regions observed in forward simulations (Figs. 4(b) and 4(e)) are consistently narrower than those in backward simulations (Figs. 4(c) and 4(f)), highlighting path-dependent behavior. Furthermore, hysteresis phenomena are absent at minimal k_2 values but emerge and intensify with increasing k_2, characterized by both a widening hysteresis width and a systematic leftward shift (toward lower k_1) of the hysteresis loop. The coherence between results from the order parameter (upper panels) and standard deviation (lower panels) subfigures reinforces the pivotal role of higher-order interactions in enabling explosive synchronization and shaping the observed hysteresis dynamics.

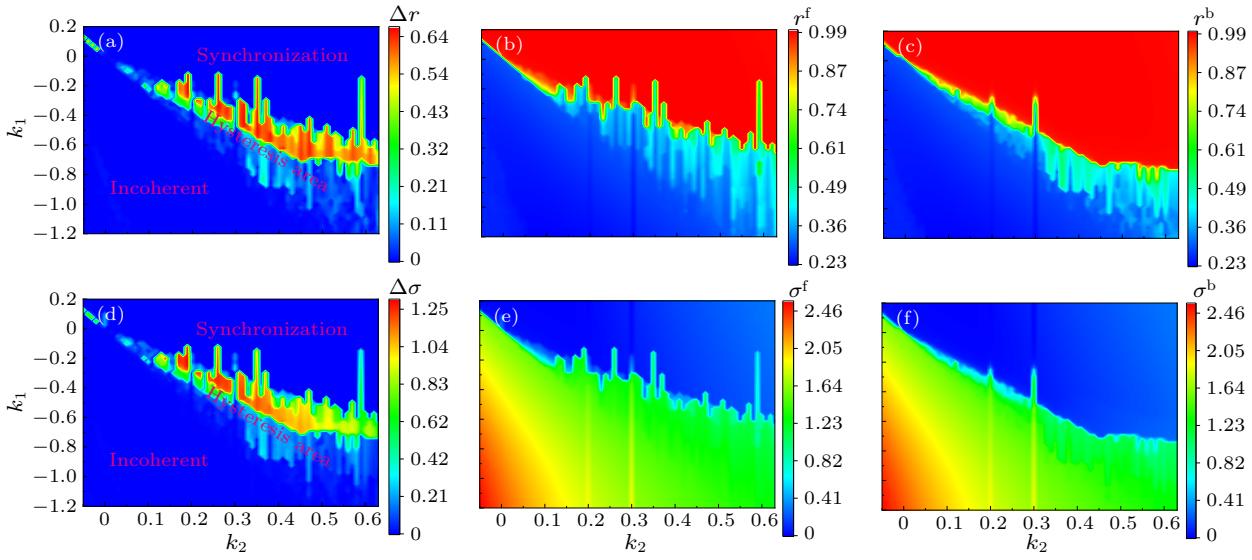


Fig. 4. Phase diagrams of the order parameter r and standard deviation σ as functions of coupling strengths k_1 and k_2. (a) and (d) Parameter space differences $(\Delta r, \Delta\sigma)$ between backward and forward simulations, (b) and (e) Forward simulation results $(r^{\mathrm{f}}, \sigma^{\mathrm{f}})$, (c) and (f) Backward simulation results $(r^{\mathrm{b}}, \sigma^{\mathrm{b}})$. In panels (a) and (d), the hysteresis area (non-zero values) is bounded by the incoherent regime (lower k_1) and synchronization regime (higher k_1). For r-based diagrams (b) and (c), synchronization regions are marked in red, with incoherent regimes elsewhere; for σ-based diagrams (e) and (f), synchronization regions appear in blue, surrounded by incoherent regimes.

To verify whether the observed phenomena are related to finite-size effects, we investigated the synchronization transition under varying system sizes. As shown in Fig. 5, changes in the number of oscillators within the system only induce minor qualitative modifications to the transition process. Meanwhile, the explosive synchronization and the persistence of hysteresis in the system remain robust. This indicates that the synchronization transition exhibits resilience to stochastic fluctuations even in small-scale systems with higher-order interactions (despite the system already containing a substantial number of triadic interactions).

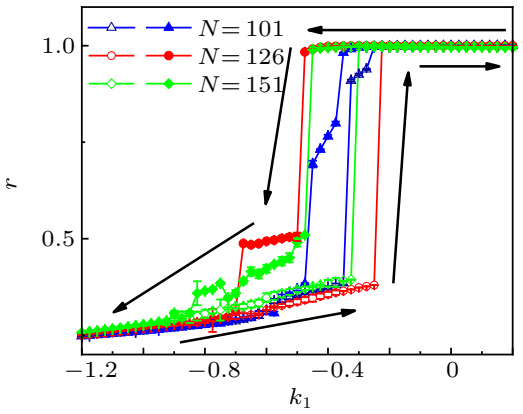


Fig. 5. Robust explosive synchronization with hysteresis across different system sizes in networks incorporating higher-order interactions. All other parameters are the same as those in Fig. 2.

In the above studies, we did not consider noise terms; however, real-world complex systems are often subject to stochastic disturbances. Therefore, we further investigated the impact of noise on explosive synchronization in higher-order complex networks. By fixing $k_2 = 0.35$ and selecting noise intensities $D = 0$, 10^{-5}, 5×10^{-5}, and 5×10^{-2}, we plotted the standard deviation σ as a function of the pairwise interaction strength k_1 (see Fig. 6).

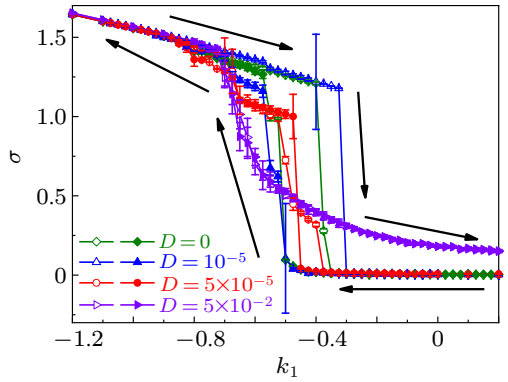


Fig. 6. When considering the influence of noise, the standard deviation as a function of pairwise interaction strength. The green, blue, red, and purple curves correspond to noise intensities of 0, 0.00001, 0.00005, and 0.05, respectively. The higher-order interaction strength is fixed at 0.35, with all other parameters unchanged.

The results reveal that when $D = 10^{-5}$, the hysteresis width slightly increases compared to the noise-free case ($D = 0$). However, as the noise intensity further increases, the hysteresis width gradually narrows, and the bistable characteristics are partially disrupted. When the noise intensity reaches $D = 5 \times 10^{-2}$, the hysteresis phenomenon vanishes entirely, and the transition between synchronization and incoherent states becomes a continuous phase transition. These findings demonstrate that explosive synchronization and hysteresis remain stable under weak noise but are destroyed under strong noise. This reveals that noise weakens the bistability induced by higher-order interactions through perturbing system states, providing important insights into the robustness analysis of synchronization behavior in real-world complex systems.

4. Summary

This paper constructs a higher-order FHN neural network model incorporating pairwise (1-simplexes) and triadic (2-simplexes) interactions, along with the Rosenzweig–MacArthur nonlinear coupling mechanism. The study systematically investigates how higher-order interactions modulate explosive synchronization and hysteresis phenomena. Based on numerical simulations, the dynamic evolution of the order parameter and standard deviation was systematically analyzed as a function of interaction strength, revealing that the introduction of higher-order interactions induces pronounced bistability within specific parameter regimes. Specifically, increasing pairwise coupling triggers an abrupt synchronization transition from incoherence to synchrony at a critical forward threshold (e.g., $k^{c}_{1,f} = -0.35$), while decreasing coupling initiates a reverse transition to incoherence at a distinct backward critical point (e.g., $k^{c}_{1,b} = -0.45$), forming a hysteresis loop. Enhanced higher-order interactions broaden the hysteresis width and reduce both forward and backward critical thresholds, underscoring their pivotal role in mediating explosive synchronization. Spatiotemporal patterns demonstrate that steady-state selection within the hysteresis regime depends strongly on initial conditions, confirming the intrinsic bistable dynamics, while phase diagrams explicitly delineate the synergistic amplification of synchronization and hysteresis by higher-order interactions. Notably, these phenomena exhibit robustness to system size variations, with hysteresis persisting across scales. Under weak noise ($D \ll 1$), bistability remains stable, whereas strong noise disrupts the hysteresis loop by destabilizing synchronized states, reverting the transition to a continuous process.

This study uncovers the mechanisms of abrupt transitions in collective behaviors within complex systems from a higher-order network perspective. It offers a theoretical framework for understanding dynamic regulation in real-world phenomena like epileptic burst synchronization in neural networks and coordinated behaviors in ecological populations.

Future research might incorporate topological data from real-world brain or ecological networks to investigate the effects of higher-dimensional simplexes or extend to heterogeneous higher-order network models with adaptive coupling. This would deepen our understanding of synchronization in multiscale complex systems. Such approaches would bridge theoretical insights with empirical observations, providing innovative strategies for controlling pathological synchrony in biological systems and optimizing collective dynamics in ecological communities.

Acknowledgement

Project supported by the National Natural Science Foundation of China (Grant No. 12404233).

References

[1] Watts D J and Strogatz S H 1998 *Nature* **393** 440
[2] Strogatz S H 2001 *Nature* **410** 268
[3] Iacopini I, Petri G, Barrat A and Latora V 2019 *Nat. Commun.* **10** 2485
[4] Muolo R, Gallo L, Latora V, Frasca M and Carletti T 2023 *Chaos, Solitons and Fractals* **166** 112912
[5] Barabasi A L and Albert R 1999 *Science* **286** 509
[6] Boccaletti S, Latora V, Moreno Y, Chavez M and Hwang D U 2006 *Phys. Rep. -Rev. Sec. Phys. Lett.* **424** 175
[7] Arenas A, Díaz-Guilera A, Kurths J, Moreno Y and Zhou C S 2008 *Phys. Rep. -Rev. Sec. Phys. Lett.* **469** 93
[8] Dorogovtsev S N, Goltsev A V and Mendes J F F 2008 *Rev. Mod. Phys.* **80** 1275
[9] Boccaletti S, Kurths J, Osipov G, Valladares D L and Zhou C S 2002 *Phys. Rep.-Rev. Sect. Phys. Lett.* **366** 1
[10] Dai X, Li X, Guo H, Jia D, Perc M, Manshour P, Wang Z and Boccaletti S 2020 *Phys. Rev. Lett.* **125** 194101
[11] Boccaletti S, Almendral J A, Guan S, Leyva I, Liu Z, Sendina-Nadal I, Wang Z and Zou Y 2016 *Phys. Rep.-Rev. Sect. Phys. Lett.* **660** 1
[12] Bayani A, Jafari S and Azarnoush H 2022 *Chin. Phys. B* **31** 020504
[13] Gómez-Gardeñes J, Gómez S, Arenas A and Moreno Y 2011 *Phys. Rev. Lett.* **106** 128701
[14] Xu T L, Guan S G, Liu Z H and Zou Y 2024 *Chaos, Solitons and Fractals* **180** 114455
[15] Zhang Y Q and Lei Y M 2024 *Chin. Phys. B* **33** 038201
[16] Skardal P S and Arenas A 2020 *Commun. Phys.* **3** 218
[17] Liu B, Zeng Y J, Yang R M and Lü L Y 2024 *Acta Phys. Sin.* **73** 128901 (in Chinese)
[18] Rosas F E, Mediano P A M, Luppi A I, Varley T F, Lizier J T, Stramaglia S, Jensen H J and Marinazzo D 2022 *Nat. Phys.* **18** 476
[19] Chen W, Liu L and Liu G P 2023 *IEEE Trans. Smart Grid* **14** 701
[20] Zolkin A L, Losev A N, Gridina D V and Aygumov T G 2021 *IOP Conf. Ser.: Mater. Sci. Eng.* **1047** 012106
[21] Lung R I, Gaskó N and Suciu M A 2018 *Scientometrics* **117** 1361
[22] Courtney O T and Bianconi G 2017 *Phys. Rev. E* **95** 062301
[23] Stehlé J, Voirin N, Barrat A, Cattuto C, Isella L, Pinton J F, Quaggiotto M, Van Den Broeck W, Régis C, Lina B and Vanhems P 2011 *PLoS One* **6** e23176
[24] Mastrandrea R, Fournet J and Barrat A 2015 *PLoS One* **10** e0136497
[25] Levine J M, Bascompte J, Adler P B and Allesina S 2017 *Nature* **546** 56
[26] Bick C, Gross E, Harrington H A and Schaub M T 2023 *SIAM Rev.* **65** 686
[27] Gambuzza L V, Di Patti F, Gallo L, Lepri S, Romance M, Criado R, Frasca M, Latora V and Boccaletti S 2021 *Nat. Commun.* **12** 1255
[28] Battiston F, Cencetti G, Iacopini I, Latora V, Lucas M, Patania A, Young J G and Petri G 2020 *Phys. Rep.-Rev. Sect. Phys. Lett.* **874** 1
[29] Anwar M S and Ghosh D 2023 *SIAM J. Appl. Dyn. Syst.* **22** 2054
[30] Anwar M S and Ghosh D 2022 *Chaos* **32** 033125
[31] Benson A R, Gleich D F and Leskovec J 2016 *Science* **353** 163
[32] Ghorbanchian R, Restrepo J G, Torres J J and Bianconi G 2021 *Commun. Phys.* **4** 120
[33] Cai Z K, Xu C and Zheng Z G 2021 *Acta Phys. Sin.* **70** 220501 (in Chinese)
[34] Wang X B, Xu C and Zheng Z G 2020 *Acta Phys. Sin.* **69** 170501 (in Chinese)
[35] Asche F, Garlock T M, Anderson J L, Bush S R, Smith M D, Anderson C M, Chu J J, Garrett K A, Lem A, Lorenzen K, Oglend A, Tveteras S and Vannuccini S 2018 *Proc. Natl. Acad. Sci. USA* **115** 11221
[36] Wang H, Ma C, Chen H S, Lai Y C and Zhang H F 2022 *Nat. Commun.* **13** 3043
[37] Civilini A, Sadekar O, Battiston F, Gomez-Gardenes J and Latora V 2024 *Phys. Rev. Lett.* **132** 167401
[38] Li J, Li W Q and Jin Z 2018 *Math. Biosci.* **297** 12
[39] Smith L D and Liu P 2024 *Phys. Rev. E* **109** L022202
[40] Xu C, Zhai Y, Wu Y G, Zheng Z G and Guan S G 2023 *Chaos, Solitons and Fractals* **170** 113343
[41] Millan A P, Torres J J and Bianconi G 2020 *Phys. Rev. Lett.* **124** 218301
[42] Sacu I E 2024 *Cogn. Neurodyn.* **18** 1877
[43] Li T Y, Yu D, Wu Y, Ding Q M and Jia Y 2024 *Eur. Phys. J. Spec. Top.* **233** 797
[44] Yang D S, Wang H, Ren G J, Yu Y G and Zhang X L 2025 *Appl. Math. Comput.* **497** 129363
[45] Skrzypek L and You Y C 2021 *Appl. Math. Comput.* **388** 125545
[46] Wang X Y and Ren X L 2011 *Chin. Phys. Lett.* **28** 050502
[47] He Z Y and Zhou Y R 2011 *Chin. Phys. Lett.* **28** 110505
[48] Yuan G Y, Yang S P, Wang G R and Chen S G 2005 *Acta Phys. Sin.* **54** 1510 (in Chinese)
[49] Chen H S, He G, Huang F, Shen C S and Hou Z H 2013 *Chaos* **23** 033124
[50] Zhao N N and Zhang X X 2023 *Physica A* **622** 128803
[51] Wang Z, Chen M, Xi X, Tian H G and Yang R 2024 *Eur. Phys. J.-Spec. Top.* **233** 779
[52] Ghosh R, Verma U K, Jalan S and Shrimali M D 2024 *Chaos* **34** 061101
[53] Rosenzweig M L and MacArthur R H 1963 *American Naturalist* **97** 209